# Bias-field dependence of the spatiotemporal evolution of magnetization reversal in a mesoscopic $Ni_{80}Fe_{20}$ element

B. C. Choi, G. E. Ballentine, M. Belov, and M. R. Freeman
*Department of Physics, University of Alberta, Edmonton, Alberta, Canada T6G 2J1*
(Received 12 April 2001; published 19 September 2001)

Ultrafast magnetization reversal dynamics in a $Ni_{80}Fe_{20}$ microstructure (10 $\mu$m by 2 $\mu$m in size and 15 nm thick) is studied using time-resolved scanning Kerr microscopy. The temporal evolution of the magnetization reversal reveals a dramatic reduction in switching time, when a steady transverse biasing field accompanies the pulsed longitudinal switching field applied to the sample. According to the analysis of time-domain images, it is concluded that the abrupt change of the switching time is due to a change in the magnetization reversal mode: the nucleation dominant reversal process is replaced by quasicoherent domain wall motion in the presence of an additional transverse biasing field. The experimental data are compared to results from micromagnetic modeling, based on the Landau-Liftshitz-Gilbert equation. The observed distinct magnetization reversal behaviors dependent on applied field conditions are well reproduced in the simulations.

DOI: 10.1103/PhysRevB.64.144418 PACS number(s): 75.60.Ch, 75.70.Ak, 75.70.Kw, 78.20.Ls

## I. INTRODUCTION

Magnetization reversal dynamics in thin continuous films on short time scales is different in many aspects from the static case.[1,2] Moreover, the reversal dynamics in small patterned elements has little relation to that in continuous films due to the magnetostatics of element edges, thus modifying the equilibrium states of the element in terms of the magnetic moment distribution.[3,4] From a practical point of view, understanding reversal dynamics on nano-and picosecond time scales in small elements with dimensions in the micrometer size regime and below has become crucial, owing to the increasing demands on conventional storage technologies and for newer approaches such as magnetic random access memories (MRAM).[5,6] Motivated by all of these accumulated interests, reversal behavior in micro- and nanosized magnets is being actively studied by a number of groups.[7–14]

In order to elucidate reversal dynamics in small elements, direct observations of magnetization reversal processes are most desirable. Imaging of micromagnetic domain structures has been carried out by magnetic force microscopy (MFM),[15] Lorentz transmission electron microscopy,[16] and ballistic electron magnetic microscopy,[17,18] in addition to magneto-optic microscopy.[19] These techniques provide good spatial resolution, but are generally focussed on the static magnetic imaging. For the study of magnetization reversal dynamics, it has been demonstrated that very high spatiotemporal resolution can be achieved by employing stroboscopic scanning Kerr microscopy with pulse excitation.[20–23] This technique is a powerful tool for dynamic micromagnetic imaging in small structures.

## II. EXPERIMENT

The sample in the present study is a 15 nm thick $Ni_{80}Fe_{20}$ rectangular element with a dimension of 10 $\mu$m$\times$2 $\mu$m. The magnetic microstructure was fabricated by electron beam lithography and lift-off techniques on a 20 $\mu$m wide Au transmission line. The $Ni_{80}Fe_{20}$ film was sputter deposited onto 300 nm thick Au on sapphire, at a growth rate of 0.1 nm/s in a system with a base pressure of $5\times10^{-8}$ torr. AFM images of the completed structure show a very smooth surface with minor burrs at the sample edge.[24] A uniaxial magnetic anisotropy was induced by applying a 12 kA/m magnetic field in the plane of the substrate during the deposition. The long geometric axis of the sample defined by patterning is aligned with its magnetic easy axis. MFM measurement of the remanent state confirmed a demagnetized domain structure consistent with the expected magnetic easy axis alignment.

Magnetization reversal dynamics are recorded by time-resolved scanning Kerr microscopy (TR-SKM). Experimental arrangements are based on a scanning Kerr microscope, including ultrafast solid-state laser and optics, a piezo-driven flexure stage for rastering the sample, and electronics controlling the time-delay of probe beam and magnetic pulse generation. A mode-locked Ti-sapphire femtosecond laser used as the light source synchronously triggers the current pulses. The laser beam is a train of 70 fs, 800 nm pulses selected at a repetition rate of at 0.8 MHz. An average optical power of 35 $\mu$W is focused onto the sample through a microscope objective. The spatial resolution ($d$) is determined by the numerical aperture (N.A.) of the objective lens and wavelength ($\lambda$) of the laser beam, given by the diffraction limited Rayleigh criterion, $d=(0.82\lambda)/\text{N.A.}$ In our experimental setup, a spatial resolution down to 0.9 $\mu$m is yielded using the 0.75 N.A. microscope objective. The computer-controlled piezostage provides scanning motion at a typical scan rate of 8 pixels/s (corresponding to 0.3 $\mu$m/s). After the probe beam is reflected from the sample, magnetization measurements are accomplished through the polarization analysis of the reflected light in an optical bridge.[25] A particular detection method using quadrant photodiodes (QPD) has been recently developed to allow for simultaneous detection of all three magnetization components (i.e., vector magnetometry).[23]

The geometric configuration of biasing and switching magnetic fields used is schematically shown in Fig. 1, where the stripe line carries a current pulse launched by a pulse

 

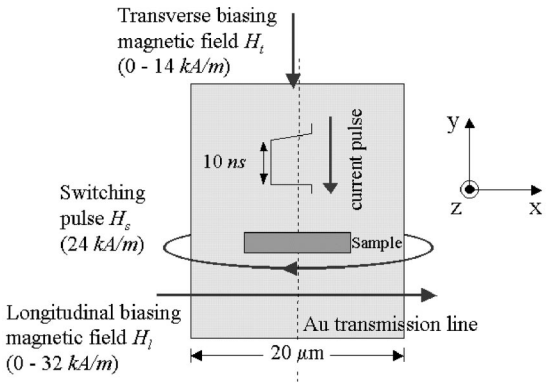


FIG. 1. Schematic measurement configuration of a 180° dynamic magnetization reversal experiment for microstructure excitation. $H_s$, $H_l$, and $H_t$ indicate the switching field, longitudinal (easy-axis) biasing field, and transverse (hard-axis) biasing field, respectively.

generator in order to create an in-plane switching field ($H_s$) of 24 kA/m along the long axis of the sample, with 0.5 ns rise time, 1.5 ns fall time, and 10 ns duration.[12] The sample is first magnetically saturated in the easy axis direction, parallel to the long sides of the elements, by an in-plane static biasing field ($H_l = 0-32$ kA/m). An in-plane switching field pulse ($H_s = 24$ kA/m) is then applied in the opposite direction to $H_l$ in order to flip the magnetization direction. The element is optically interrogated while switching is taking place. Additionally, an in-plane static transverse biasing field $H_t$ can be applied along the hard axis of the sample to manipulate the magnetization reversal process.

### III. RESULTS

Time-resolved magneto-optic Kerr effect measurements were made with the 0.9 $\mu$m focus spot positioned at the center of the structure. In Fig. 2 the time traces of easy axis

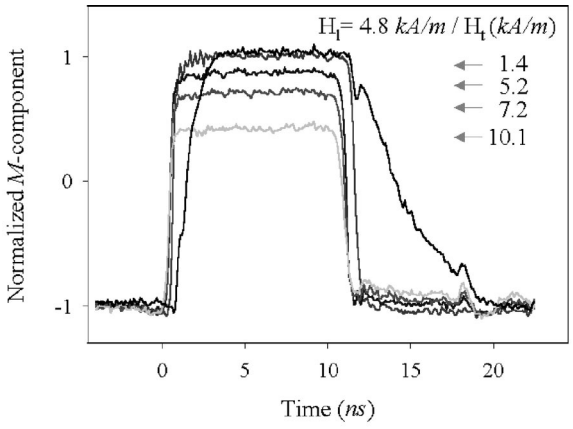


FIG. 2. Temporal evolution of easy axis magnetization components in different transverse biasing fields, while longitudinal biasing field is being held fixed at $H_l = 4.8$ kA/m. The thick line indicates the magnetization component measured at $H_t = 0$ kA/m. The beginning of the pulse corresponds to 0 ns. Small peaks found in the back reversal occur due to electrical reflections in the magnetic pulse line.

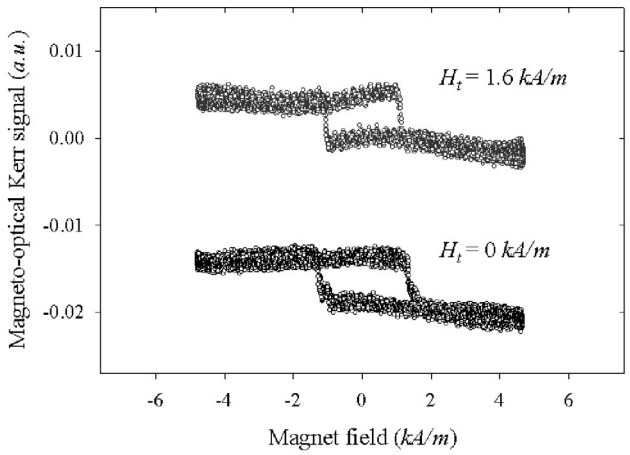


FIG. 3. MOKE hysteresis loops measured on the element for two different transverse fields; $H_t = 0$ and 1.6 kA/m. A decrease of the coercive field from 1.3 kA/m to 1.0 kA/m is measured with the increase in the loop squareness by applying an additional transverse biasing field.

magnetization components are compared for different transverse biasing fields $H_t$, while $H_l$ is kept at 4.8 kA/m. Applying no transverse field, i.e., $H_t = 0$ kA/m as indicated by the thick line, a definite delay in the magnetic response after the beginning of the pulse is observed, and the subsequent dynamics are relatively slow with the magnetization fully reversed after 3.5 ns. A striking change in the magnetic response is observed when a transverse bias field $H_t$ is applied perpendicular to the easy axis. In such cases the magnetic response becomes much faster with respect to the case without applying $H_t$, and the magnetization switches within 1 ns after the pulse is given. A field strength as low as $H_t = 1.4$ kA/m is found to be sufficient to cause such an abrupt switching. The qualitative explanation for this effect is that when a transverse biasing field $H_t$ is applied, the equilibrium position of the magnetization vector $\boldsymbol{M}$ is away from the initial easy axis, hence the reversing field exerts torque on the magnetization vector immediately. In addition, the magnetization is away from the minimum anisotropy energy state along the easy axis, so the effective coercive field is lower than for $H_t = 0$ kA/m. Consequently, lower longitudinal Zeeman energy or smaller switching field strength is required to overcome the energy barrier.[26] The results in Fig. 2 thus provide a direct exploration of how the dynamic switching time is sensitively determined by the time-dependent torque acting on $\boldsymbol{M}$ during its entire excursion.

The change in the reversal mechanism in the presence of the additional transverse biasing field is also reflected in ''quasistatic'' magneto-optic Kerr effect (MOKE) measurements. During measurements the laser beam is focused at the sample center, and the external magnetic field is swept at a constant rate of 1 kA/m s. Figure 3 shows hysteresis curves measured on the element with and without applying transverse field. For example, we observed a decrease of the coercive field from 1.3 kA/m to 1.0 kA/m, with an increase in the loop squareness, when a transverse biasing field $H_t = 1.6$ kA/m was present. This result is also suggestive that distinct microscopic magnetization reversal mechanisms oc-

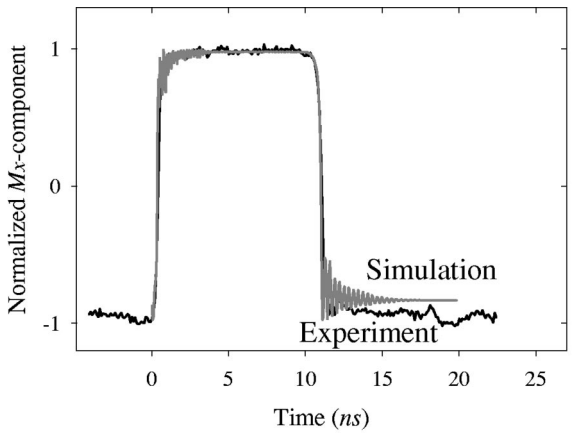


FIG. 4. Comparison of the temporal evolution of the easy axis magnetization component simulated for the biasing field conditions of $H_t = 5.2$ kA/m and $H_l = 4.8$ kA/m to the experimental time trace. Expanded views for the rising and falling ends of the switching are shown in Fig. 5.

cur in different biasing-field conditions, and can be correlated with the drastic change in the time traces observed in Fig. 2. In particular, the decrease of $H_c$ can be understood by the initial deviation of the magnetization vectors from the easy axis at a given $H_t$. Therefore, at $H_t \neq 0$ kA/m a new energy minimum is formed at which the energy barrier is reduced to zero height by a lower external field compared to the case for $H_t = 0$ kA/m.

For comparison of experimental temporal evolution of the magnetization reversal with a model, we resort to a numerical approximation of the Landau-Liftshitz-Gilbert (LLG) equation[27]

$$\frac{dM}{dt} = \gamma[\boldsymbol{M} \times \boldsymbol{H}^{\text{eff}}] - \alpha\gamma[\boldsymbol{M} \times (\boldsymbol{M} \times \boldsymbol{H}^{\text{eff}})], \qquad (1)$$

where $\gamma$ is the gyromagnetic ratio and $\alpha$ is the dimensionless damping parameter. The simulation is a time domain finite element integration of the LLG equation, under the assumption that the effective field $\boldsymbol{H}^{\text{eff}}$ is produced by the exchange, magnetostatic, crystalline anisotropy, and Zeeman (external field) energies of the magnetization. The sample is broken into a two dimensional array of 512 by 128 blocks making cells $19.5 \times 15.6 \times 15$ nm$^3$ each. Micromagnetic calculations have been carried out at 0 K. We note that the Curie temperature of the element is much higher than room temperature, allowing a low-temperature approximation in the statistical mechanical sense.[28]

The temporal evolution of the easy axis magnetization component simulated for the biasing field conditions of $H_t = 5.2$ kA/m and $H_l = 4.8$ kA/m is compared to the experiment in Fig. 4. The simulated time trace is averaged over an area with the diameter of 0.9 $\mu$m at the center in the element, reflecting the experimental condition. The simulation agrees remarkably well with the experiment even in the absolute time scale. Since the time traces for the experiment and simulation mostly overlap, expanded views for the rising and falling ends of the switching are shown in Fig. 5. From the comparison, the experimental traces are found to be

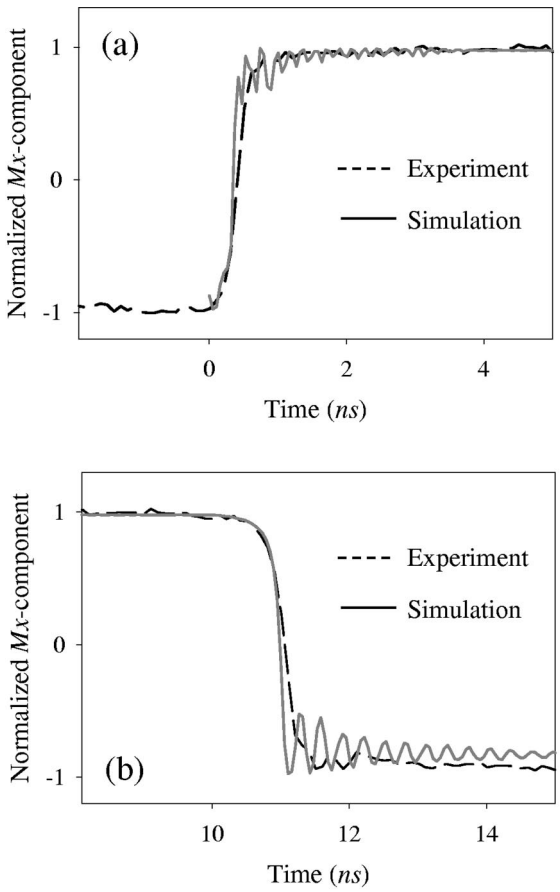


FIG. 5. Expanded views for the rising (a) and falling (b) ends of the time traces shown in Fig. 4. The small oscillations seen in the rising and falling ends are due to magnetization precession as reported previously (Ref. 12).

slightly lagging behind, with the initial and final slopes steeper in the simulation. Noticeable in the simulation are small oscillations found both in the rising and falling ends. These are on account of the precessional motion of the magnetization vector as reported previously,[12] and are less pronounced in the experiment due to the experimental temporal resolution limited by the $\sim 50$ ps RMS jitter of delay generator electronic (Stanford Research Systems DG535). The overall agreement of the micromagnetic simulations to the experimental result demonstrates the micromagnetic modeling using LLG equations is capable of describing the magnetization reversal dynamics in small magnetic elements.

More detailed insight into the temporal evolution of the magnetization reversal is obtained by direct time-domain imaging. The left column of Fig. 6 shows a sequence of time-resolved images representing the easy axis magnetization components for $H_t = 5.2$ kA/m and $H_l = 4.8$ kA/m at selected time points, demarcated in nanoseconds relative to the initial application of the switching pulse. The images are on a linear gray scale to render the change in magnetization components with black corresponding to no change and white corresponding to the saturation level or maximum possible reversal. Imaging reveals that edge domains associated with demagnetized regions at the short ends are formed ($t = 0.3$ ns), and then these edge domains propagate in the

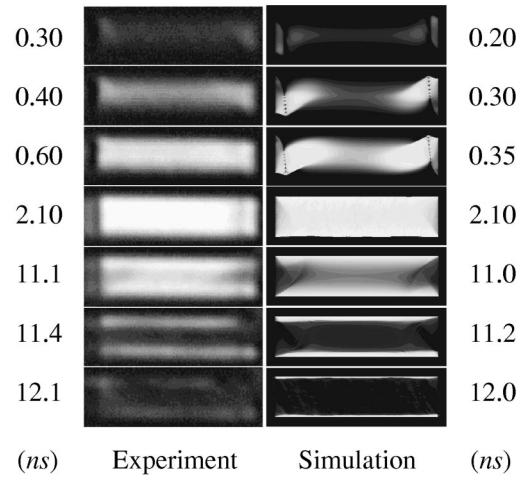


FIG. 6. Spatial magnetization profiles for experiment and simulation as a function of time after the magnetic pulse was applied. The biasing field conditions are the same as for Fig. 4. Each panel corresponds to a 12 $\mu$m$\times$4 $\mu$m field of view. The numbers by the frames indicate the time in nanoseconds at which the measurement was made, relative to the initial application of the switching pulse.

direction of the easy axis and merge to form a long narrow domain parallel to the easy axis ($t=0.4$ ns). In the next stage, the elongated domain expands by parallel shifts in the hard direction to reach the long edge ($t=0.6$ ns) until saturation is reached ($t=2.1$ ns). On the back reversal process, the pinning of the reversal along the long edges is very pronounced ($t=11.1$–$12.1$ ns). This lateral edge pinning is attributed to the delay of the magnetization reversal due to domain walls forming along the lateral sides of the element. These experimentally obtained time domain images are compared to those obtained by the simulation. The right column in Fig. 5 shows the simulated time domain images along the easy axis for the same biasing field strengths used in experiment. In remarkable agreement with the experiment, short edges of the sample initiate reversal ($t=0.20$ ns) and then propagate toward the center until the saturation reaches ($t=0.3$–$2.1$ ns). Quite similar to the experimental case, the long edges are found to remain pinned along the initial magnetization direction ($t=11.1$–$11.2$ ns) and are reversed last ($t=12.0$ ns). From the experimental and simulated time domains, it is concluded that the fast dynamic reversal in this case proceeds via a quasicoherent magnetization reversal, also represented by a characteristic domain wall motion.[19]

The ''simpler'' experimental condition, i.e., without including the additional transverse biasing field $H_t$, yields a far more complex response. In this case the dynamics respond strongly to many subtle influences, and significant discrepancies are found between the experiment and the model. Figure 7 compares the simulation and experiment for $H_t=0$ kA/m and $H_l=4.8$ kA/m. For the front reversal, the saturation is reached much faster ($\sim 2.0$ ns) in the simulation, with the experimental time trace considerably lagging behind. This faster switching is in line with the lack of the long tail in the simulated back reversal. From comparison with additional simulated results,[29] it can be concluded that the relatively delayed magnetic response in experiment implies that crystalline, patterning, and thermal ''imperfections'' in the sample, are involved in the reversal process to slow down the observed magnetic response. It is of great interest to note that such a delay in magnetic response is easily avoided *in the same sample* by applying the transverse biasing field, as shown above in Fig. 4.

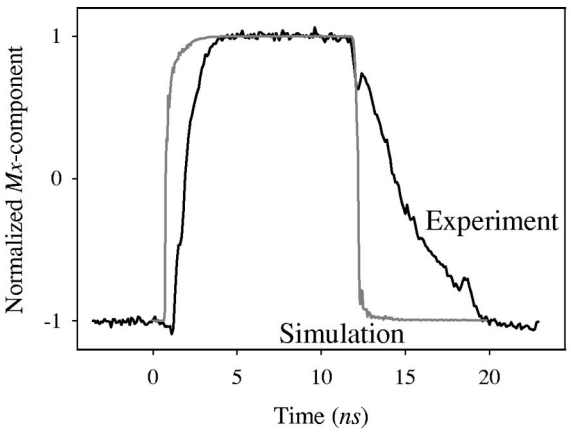


FIG. 7. Comparison of the temporal evolution of the easy axis magnetization component between the simulation and experiment for $H_t=0$ kA/m and $H_l=4.8$ kA/m.

Another aspect in Fig. 7 is the asymmetric trace profiles between front and back reversal both in the experiment and simulation. Refraining from considering the sample imperfections, this asymmetry can principally be accounted for by the different driving field strengths in front and back reversal. For the experiment shown in Fig. 7, $H_s=24$ kA/m is applied combined with $H_l=4.8$ kA/m, thus the net driving field strengths are 19.2 kA/m and 4.8 kA/m for the front reversal and back reversal. Under these field conditions the experimental switching times, $\tau_s$, are measured 1.6 ns and 7.3 ns for front and back switching, defining $\tau_s$ as the interval for 10% to 90% of the total magnetization change. From the simulated time traces, $\tau_s$ is determined 0.7 ns and 0.9 ns for front and back switching. In comparison with earlier works,[30,31] $\tau_s$ is roughly consistent with the prediction models in which $\tau_s$ is roughly inversely proportional to the net switching field $H_s^{\text{net}}$,

$$\tau_s = \frac{S_w}{H_s^{\text{net}}}, \tag{2}$$

where $S_w$ is a switching coefficient in which all of the detail is buried. Figure 8 plots $1/\tau_s$ as a function of $H_s^{\text{net}}$ for the front and back switching measured from the experiment and simulation with various field strengths. From all data, the switching time $\tau_s$ is found to decrease for $H_s^{\text{net}}$ increasing, and approximately linear relations between $1/\tau_s$ and $H_s^{\text{net}}$ are found. For the front switching $S_w$ is determined to be about 30 A $\mu$s/m (experiment) and 13 A $\mu$s/m (simulation), but the inverse relation is not strictly obeyed over a broader field range. The discrepancy in $S_w$ between experiment and simulation suggests the possible modification of the switching coefficient due to imperfections in real microscopic samples

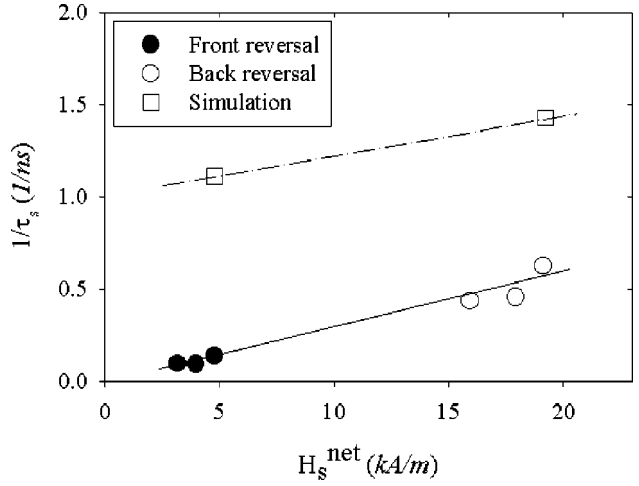


FIG. 8. Inverse switching time $1/\tau_s$ as a function of net switching field $H_s^{\text{net}}$ measured from experiments and simulation. Switching time $\tau_s$ is defined as the interval for 10% to 90% of the total magnetization.

and thermal fluctuations, which might be more important in the switching process without applying transverse bias field.

An examination of time domain images is very instructive in the case of the fully different reversal mechanism observed when no transverse biasing field $H_t$ is applied during the reversal experiment. The left column of Fig. 9 shows time domain images representing the easy axis magnetization component during switching in the presence of $H_l = 4.8$ kA/m, but with $H_t = 0$ kA/m. In this case, the initial stage of the magnetization reversal is found to be governed by the magnetostatics of the short edges, with the small initial domain nuclei precipitating the formation of a stripe-like structure inside the sample, from which reversed domains are

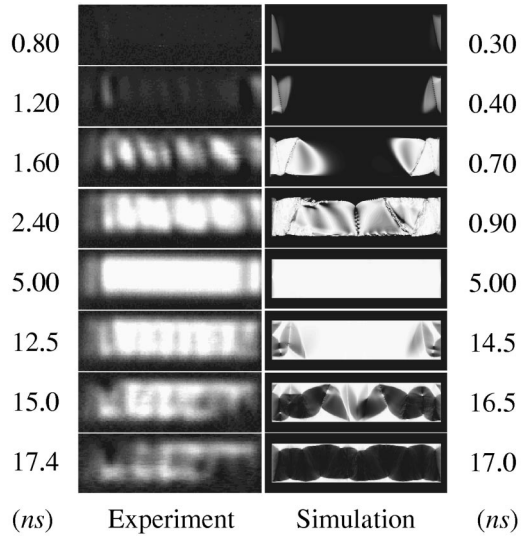


FIG. 9. Spatial magnetization profiles for experiment and simulation as a function of time after the magnetic pulse was applied, for the case of pure parallel-antiparallel reversal. The applied longitudinal biasing field is $H_l = 4.8$ kA/m, with no applied transverse biasing field.

grown ($t = 0.8$ and 1.2 ns). This stripe instability is in the directions perpendicular to the applied field and is very regular with a periodicity of $\sim 1.35$ $\mu$m both in front and back reversal. The reversed domain regions expand gradually ($t = 1.6$ and 2.4 ns) and finally merge to create a uniform distribution of fully reversed magnetization ($t = 5$ ns), excluding the left and right edge free magnetic poles. During the entire course of this reversal, the ultimate speed-limiting factor of the switching process seems to be the ''punch-through'' mechanism of the 360° domain walls which form when the stripe regions come together. Back reversal proceeds also via the formation of the stripe domains ($t = 12.5$ ns), and the lateral edge pinning occurs along the long edges of the sample ($t = 15$ and 17.4 ns). In the simulation (right column in Fig. 9), the formation of the stripe-like instability can also be identified in the directions perpendicular to the applied. The simulated magnetization reversal is mainly governed by the formation of edge domains on the short ends and the reversal proceeds in a zigzag pattern across the sample until it meets in the center ($t = 0.9$ ns). This reversal mechanism appears to differ from the experimental observation, where the magnetization reversal proceeds by gradual growth of a more regular and orthogonal set of quasiperiodic domain nuclei. Nevertheless, the simulation is qualitatively in good agreement, at the level of reproducing the characteristic reversal behavior described here as stripe domain nucleation.

## IV. CONCLUSIONS AND DISCUSSION

For the pure parallel/antiparallel reversal, with all fields applied along the easy axis of the rectangle, it is found that the formation of the stripe-like instability is the main micromagnetic feature describing the nature of the magnetization reversal and limiting the magnetic response. The micromagnetic simulation is consistent with the experimental observations, and implies that the nucleation of stripe domains inside the sample is a preferred metastable local energy minimum state before a full magnetization reversal is reached. Such a metastable state can be easily bypassed by applying a hard axis bias field. Then the reversal process is dictated by a quasicoherent magnetization reversal, where the reversed domains grow from the short edges of the element and propagate toward the element center. This reversal mechanism in particular is quantitatively reproduced in numerical simulations, demonstrating the validity of dynamic micromagnetic modeling based upon the LLG equation. This is also an important result from the application point of view, since it is desirable that the magnetic elements switch by a simple magnetization reversal process in the absence of many domains midway through reversal process.

A challenging question in the present experiment is whether the entire dynamics presented here is perfectly repeatable, since the stroboscopic scanning technique by its nature captures only the repetitive part of the process being imaged. Nonrepetitive instabilities, such as thermal fluctuation of the individual spins, will lead to the averaging the temporal response. In addition to varying scan rate, number of averages, etc., the most sensitive test for underlying sto-

chastic behavior so far comes from spectrum analysis of the noise on the magneto-optic signal.[32] In the present experiments, evidence of additional random behavior has not been observed, that is, the random components present are at too small a level to detect. Nevertheless there is strong motivation for the development of ''single shot'' measurements of this kind.

In conclusion, we have investigated the dynamics of magnetization reversal in micrometer-sized $Ni_{80}Fe_{20}$ rectangular element, both by time-resolved imaging experiments and though comparison with micromagnetic modeling. It is found that the applied field condition greatly influences the reversal dynamics of small magnetic elements; applying a transverse biasing field $H_t$ reduces the switching time and prevents the stripe domain nuclei from growing inside the magnetic structure. This demonstrates unequivocally how the magnetization reversal mode changes sensitively in response to the switching field configuration. This is the key parameter for precise magnetization switching control.

## ACKNOWLEDGMENTS

We gratefully acknowledge support from the Natural Sciences and Engineering Research Council of Canada, the Canadian Institute for Advanced Research, and the National Storage Industry Consortium. The samples were produced at the University of Alberta MicroFab, and the experiments performed on equipment donated by Quantum Corporation. The simulations were performed using resources of the Multimedia Advanced Computational Infrastructure.

[1] S.W. Yuan and H.N. Bertram, J. Appl. Phys. **73**, 5992 (1993).
[2] B. Heinrich, Can. J. Phys. **78**, 161 (2000).
[3] A.F. Popkov, L.L. Savchenko, N.V. Vorotnikova, S. Tehrani, and J. Shi, Appl. Phys. Lett. **77**, 277 (2000).
[4] K.J. Kirk, J.N. Chapman, and C.D.W. Wilkinson, Appl. Phys. Lett. **71**, 539 (1997).
[5] J.M. Daughton *et al.*, Thin Solid Films **216**, 162 (1992).
[6] W.J. Gallagher *et al.*, J. Appl. Phys. **81**, 3741 (1997).
[7] C.H. Back, D. Weller, J. Heidmann, D. Mauri, D. Guarisco, E.L. Garwin, and H.C. Siegmann, Phys. Rev. Lett. **81**, 3251 (1998).
[8] C. Stamm, F. Marty, A. Vaterlaus, V. Weich, S. Egger, U. Maier, U. Ramsperger, H. Fuhrmann, and D. Pescia, Science **282**, 449 (1998).
[9] M. Hehn, K. Ounadjela, J.-P. Bucher, F. Rousseaux, D. Decanini, B. Bartenlian, and C. Chappert, Science **272**, 1782 (1996).
[10] R.P Cowburn, D.K. Koltsov, A.O. Adeyeye, M.E. Welland, and D.M. Tricker, Phys. Rev. Lett. **83**, 1042 (1999).
[11] A.Y. Elezzabi, M.R. Freeman, and M. Johnson, Phys. Rev. Lett. **77**, 3220 (1996).
[12] B.C. Choi, G.E. Ballentine, M. Belov, W.K. Hiebert, and M.R. Freeman, Phys. Rev. Lett. **86**, 728 (2001).
[13] Y. Acremann, C.H. Back, M. Buess, O. Portmann, A. Vaterlaus, D. Pescia, and H. Melchior, Science **290**, 492 (2000).
[14] R.H. Koch, J.G. Deak, D.W. Abraham, P.L. Trouilloud, R.A. Altman, Yu Lu, W.J. Gallagher, R.E. Scheuerlein, K.P. Poche, and S.S.P. Parkin, Phys. Rev. Lett. **81**, 4512 (1998).
[15] R.D. Gomez, T.V. Luu, A.O. Pak, K.J. Kirk, and J.N. Chapman, J. Appl. Phys. **85**, 6163 (1999).
[16] J.N. Chapman, P.R. Aitchison, K.J. Kirk, S. McVitie, J.C.S. Kools, and M.F. Gillies, J. Appl. Phys. **83**, 5321 (1998).
[17] W.H. Rippard and R.A. Buhrman, Appl. Phys. Lett. **75**, 1001 (1999).
[18] W.H. Rippard, A.C. Perrella, P. Chalsani, F.J. Albert, J.A. Katine, and R.A. Buhrman, Appl. Phys. Lett. **77**, 1357 (2000).
[19] A. Hubert and R. Schäfer, *Magnetic Domains* (Springer-Verlag, Berlin, 1999).
[20] W.K. Hiebert, A. Stankiewicz, and M.R. Freeman, Phys. Rev. Lett. **79**, 1134 (1997).
[21] T.M. Crawford, T.J. Silva, C.W. Teplin, and C.T. Rogers, Appl. Phys. Lett. **74**, 3386 (1999).
[22] G. Ju, A.V. Nurmikko, R.F.C. Farrow, R.F. Marks, M.J. Carey, and B.A. Gurney, Phys. Rev. Lett. **82**, 3705 (1999).
[23] G.E. Ballentine, W.K. Hiebert, A. Stankiewicz, and M.R. Freeman, J. Appl. Phys. **87**, 6830 (2000).
[24] J. Lohau, S. Friedrichowski, and G. Dumpich, J. Vac. Sci. Technol. B **16**, 1150 (1998).
[25] M. R. Freeman and W. K. Hiebert, in *Spin Dynamics in Confined Magnetic Structures*, edited by B. Hillebrands and K. Ounadjela (Springer-Verlag, Berlin, 2001).
[26] We note that this is well known from quasistatic studies and modeling (Ref. 19), and our study is extending to the fast dynamic regime.
[27] M. Mansuripur, J. Appl. Phys. **63**, 5809 (1988).
[28] The good agreement with finite temperature experiment can be ascribed to the relatively coherent magnetization processes (as found especially in the case with transverse bias field, Fig. 4), in which characteristic magnetic volumes of reversing regions are always large enough that the influence of thermal energy is negligible. However, the simulation result, in particular without transverse bias field (Fig. 7), reveals some discrepancy between experiment and simulation. This can be attributed to the thermal fluctuation.
[29] G.E. Ballentine *et al.* (unpublished).
[30] E.M. Gyorgy, J. Appl. Phys. **29**, 283 (1958).
[31] F.B. Humphrey, J. Appl. Phys. **29**, 284 (1958).
[32] M.R. Freeman, R.A. Hunt, and G.M. Steeves, Appl. Phys. Lett. **77**, 717 (2000).